SURFACE SHEAR STRESS MEASUREMENTS AROUND MULTIPLE JETS IN CROSSFLOW USING THE FRINGE IMAGING SKIN FRICTION TECHNIQUE

Sean D. Peterson
School of Mechanical Engineering
Maurice J. Zucrow Laboratories, Purdue University
West Lafayette, Indiana 47907 USA
sdpeterson@purdue.edu

Michael W. Plesniak
School of Mechanical Engineering
Maurice J. Zucrow Laboratories, Purdue University
West Lafayette, Indiana 47907 USA
plesniak@ecn.purdue.edu

ABSTRACT

The skin friction distribution and velocity field around multiple jets in crossflow is examined experimentally for various plenum configurations. The skin friction is determined using the Fringe-Imaging Skin Friction (FISF) technique. This technique yields both the magnitude and direction of the skin friction vectors. The velocity field in the jets, measured using Particle Image Velocimetry (PIV) is analyzed and correlated to the skin friction distribution. The counter-flow plenum case has a pronounced skin friction deficit downstream of the injection holes. The deficit is caused by the lifting of fluid away from the wall by the counter-rotating vortex pair (CRVP), which in the counter-flow case stays closer to the wall than in the co-flow case. A potential flow analysis of a pair of counter-rotating vortices above a wall demonstrates that the distance of the CRVP from the wall affects the wall pressure distribution, and hence the separation phenomena, more strongly than does the strength of the vortices.

INTRODUCTION

Modern gas turbines operate at inlet temperatures greater than the failure temperature of the turbine vane material. The turbine vanes must be cooled rather aggressively to avoid failure. One technique used to reduce vane temperatures is discrete-hole film cooling, in which cool, dense air from the compressor is supplied through internal passages in the vane. The cooler air impinges upon the internal surfaces of the vane before passing through a narrow plenum discharging through small holes in the vane surface. Once discharged, the air creates a thin coolant film over the vane surface, protecting it from the harsh environment above.

Analysis of the discrete-hole film cooling technique requires an understanding of the jet-in-crossflow (JICF). Jets in crossflow have been studied for many years, as reviewed by Margason (1993), Holdeman (1993), and Morton and Ibbetson (1996). The general flow structures, the film cooling effectiveness, and the heat transfer for a variety of injection hole geometries and plenum flow directions have been documented, e.g. see Hale (1999), Hale et al. (1999), and Hale et al. (2000). Despite the years of research however, many aspects of film cooling remain unresolved, especially for short holes; e.g. see Simoneau and Simon (1993) and Hale (1999). An issue that has received relatively little attention is the effect of the supply plenum flow on the development of the jet (see Wittig et al., 1996; Thole et al., 1997; Berhe and Patankar, 1996; and Burd and Simon, 1998a,b).

In this study, the effects of plenum flow direction (see Figure 1) on the surface shear stress distribution around a row of short film-cooling injection holes and the velocity field in the jet is examined. The term "short" refers to a length-to-diameter ratio on the order of one. The short injection hole geometry complicates the standard jet-in-crossflow problem because the flow exiting the hole is not fully developed and depends greatly on the supply plenum flow, as well as the external flow. The objective of this study is to investigate the skin friction distribution around a row of short injection holes and explain the effects of plenum flow direction on the shear stress distribution. Particle image velocimetry is used to relate the skin friction trends to flow structures in the JICF.

NOMENCLATURE

a: distance between vortices in Y direction (potential flow analysis)
b: distance between vortices in Z direction (potential flow analysis)
C_f: skin friction coefficient
D: hole diameter
L/D: hole length-to-diameter ratio
M: blowing ratio = jet bulk mean velocity/free stream velocity
n_0: index of refraction of oil
p: static pressure
q_∞: dynamic head = $\frac{1}{2} \rho U_\infty^2$

Re_θ: Reynolds number based on momentum thickness
Δs: fringe spacing
t: time
v, w: wall-normal and spanwise velocity components
X: streamwise distance downstream from hole centerline
Y: height from the test section floor
Z: spanwise distance from hole centerline
U_∞: free stream velocity
λ: wavelength of incident radiation
μ_0: dynamic viscosity of oil
ρ: air density
τ_w: shear stress
θ_r: angle of incidence
θ_0: initial boundary layer momentum thickness

EXPERIMENTAL TECHNIQUES

Experimental Apparatus

The experimental studies were performed in a low speed wind tunnel with a 122 cm long by 30 cm square, optically-clear test section (see Wolochuck et al., 1994). The specially designed test section floor served as the boundary layer plate and was equipped with a single row of five injection holes fed by a narrow plenum (see Hale et al., 2000). The blowing ratio, the hole injection angle, and the plenum flow direction are variable parameters in the study, the emphasis being on the plenum flow direction in this paper. Table 1 contains the relevant experimental parameters.

TABLE 1: EXPERIMENTAL PARAMETERS

Hole Diameter (D)	19 mm
Free Stream Velocity (U_∞)	10 m/s
Hole Length-to-Diameter Ratio (L/D)	0.66
Nominal Oil Viscosity (25°C)	8.749 cs
Incident Radiation Wavelength (λ)	542 nm
Hole Orientation	90°
Blowing Ratio (M)	0.5, 1.0
Reynolds Number (Re_θ)	1550
Initial momentum thickness (θ_0)	2.3 mm
Plenum Height	1D

Skin Friction Measurements

The Fringe-Imaging Skin Friction (FISF) technique, developed by Monson & Mateer (1993) and perfected by Zilliac (1996) and Driver (1997), was used to measure the skin friction distribution for 90° injection holes with various plenum flow directions and blowing ratios. The FISF technique is based upon the principle that an oil droplet on a surface placed in a flow will deform into a very thin film or wedge with a linear slope due to the shear forces. Since the oil film is very thin (~microns), the shear forces of the flow dominate and pressure and body forces become negligible. The slope is therefore proportional to the applied shear stress, and can be determined from interference patterns created by illuminating the oil. The oil is optically clear,

allowing some incident radiation to pass through, while reflecting the remaining light. The radiation transmitted through the oil reflects off of the boundary layer plate and interferes with the light reflected from the oil surface, creating the interference pattern. The expression for the skin friction derived by Monson and Mateer (1993) is given by equation (1).

$$C_f = \frac{\tau_w}{q_\infty} = \frac{2n_0\mu_0\Delta s}{q_\infty\lambda t}\cos(\theta_r) \tag{1}$$

In this experiment, a 12.7 cm by 40.6 cm layer of self-adhesive Monokote was adhered to the plate. Monokote was used because its index of refraction is similar to that of the oil, which is necessary to produce clear fringes. The Monokote dimensions allowed coverage of the area around two injection holes (see Figure 2). Drops of Dow Corning DC 200 oil were then applied to the surface and the wind tunnel was operated. To obtain accurate skin friction measurements, a number of parameters must be known, such as the dynamic head and oil viscosity over the entire run. The run times of the experiments were 6 minutes, during which the temperature varied by less than 1°C and thus the oil viscosity was constant. The dynamic head integrated over the tunnel run time was recorded using a pressure transducer read into a LabView VI. The oil film was illuminated with green monochromatic light produced by a custom "light-box". Green light was found to produce the clearest fringes; see Zilliac (1996). A Panasonic 768x486 pixel CCD camera captured the oil fringe images and the CXWIN4G computer application developed by Zilliac (1999) was used on a 100MHz Pentium computer to process the data and compute the skin friction vectors. The fringe clarity and thus the measurement accuracy were found to depend heavily upon particulate contamination of the oil and illumination. Dust settling upon the oil caused false fringe intensity and spacing readings. Many data were discarded because of this contamination. To combat this, the run times were kept short and the fringes were imaged as quickly as possible upon run completion. According to Zilliac (1999), the uncertainty in this technique is less than 5% when performed properly. When compared with Clauser plot and correlations in the undisturbed approach boundary layer, the FISF results agreed to within 10%.

Velocity Measurements

Particle Image Velocimetry (PIV) was used to determine the velocity distribution in the plane parallel to the injection hole as well as the plane perpendicular to the injection plane in the streamwise direction. PIV is a global velocity measurement scheme (see Adrian, 1988; Willert and Gharib, 1991; and Westerweel, 1993) whereby velocity is computed by cross-correlating a pair of particle-laden images taken a short time apart. In the

current experiments, the jets were seeded with 3 to 10 micron diameter particles produced by burning Glycol in a *Rosco 1500* Studio Fog machine. The desired planes were illuminated by a *New Wave* 35mJ/pulse Nd:YAG laser and the images were captured by a TSI PIVCam10-30 CCD array (1000x1000 pixels). One hundred image pairs were acquired for each experimental configuration, which after post processing were ensemble averaged using *TecPlot*. The *TSI Insight* software package performed the cross-correlation and vector validation. The interrogation region was 32 by 32 pixels.

RESULTS

Skin Friction Measurements

Hale (1999) and Hale et al. (1999, 2000) used surface streak visualization techniques (oil and lampblack) to visualize the flow structures and surface shear stress around 90° short injection holes, among other geometries. The results for the co-flow plenum at a blowing ratio of 1.0 are reproduced here in Figure 3. The features of interest in this figure are (1) the upstream stagnation region with horseshoe vortices, (2) the wake vortices and (3), the downstream "wake" region dominated by primary and secondary counter-rotating vortex pairs. The dark patches at the trailing edge of the injection hole are "pools" of oil marking spiral nodes of separation associated with wake vortices; see Fric & Roshko (1994). Figure 3 also depicts a topological map of the wall shear stress inferred from the oil and lampblack technique, as reported by Hale et al. (1999).

The previous work by Hale et al. provided a qualitative understanding of the wall shear stress distribution around the film-cooling holes. Figure 4 depicts the skin friction distribution and magnitude upstream, around, and downstream of two 90°-injection holes. The figure shows the calculated skin friction vectors overlaid on contours of constant shear stress. Due to the nature of the oil droplets, it was virtually impossible to place the oil on a regular grid. The oil drops were applied in pseudo-random positions and the analysis code used a triangulation scheme to form an "unstructured mesh"; see Zilliac (1999). A typical data set contains roughly 560 skin friction vectors.

The flow far upstream of the holes is unaffected by the jet and thus the skin friction is roughly uniform across the test area. The magnitude of the average skin friction coefficient is within 7% of the value computed using White's correlation (White, 1991) for a Reynolds number of 1550 for turbulent flow over a flat plate ($C_f = 0.00378$). As the flow approaches the coolant jets, the wall shear stress decreases and the flow diverts around the jet. This region of decrease corresponds with the separation nodes in the horseshoe vortex region shown in Figure 3. Slightly downstream of the hole

centerline, the magnitude of the shear stress begins to increase rapidly, as the flow is pulled into the wake vortex region. Proceeding just downstream of the hole in the "wake" region, the skin friction vector reverses direction, denoting the recirculation region. The magnitude of the shear stress here is small. Note that directly downstream of the injection holes, in the region of spiral nodes of separation, the shear stress is not sufficient to displace the oil and thus skin friction measurements cannot be obtained here. Continuing downstream, beyond the wake vortex region, the skin friction vectors again orient themselves in the direction of the flow. Those vectors in the wake region have a magnitude roughly 30% less (approximately 0.0026 on the average) than the "up-stream" vectors. This is not surprising since the crossflow boundary layer is still recovering from the jet interaction. Sufficiently far downstream of the jet, the skin friction again becomes roughly uniform, regaining the initial free stream value.

Plenum Feed Direction

For short holes, plenum feed direction drastically affects the JICF velocity field by altering the in-hole separation regions (see Brundage et al., 1999). Figure 5 shows two data sets with different plenum feed directions for a 90° injection hole geometry with a blowing ratio of M = 1.0. The most apparent effect of the plenum feed direction is the presence of a prominent skin friction deficit (SFD) downstream of the hole in the counter-flow plenum geometry (black region). This deficit continues far downstream, beyond the measurement region. Though it is not easily apparent in the plots, the magnitudes of the skin friction vectors downstream of the holes in the co-flow plenum case are also smaller than the surrounding vectors. Therefore, the SFD occurs for both co- and counter-flow geometries. The effect is simply more pronounced for the counter-flow case. The skin friction vectors outboard of the SFD region tend to point inward, suggesting that lifting of the low momentum fluid in this region causes the deficit. This flow pattern is consistent with the induced velocity field of the well-documented counter-rotating vortex pair (CRVP). PIV data acquired in a plane parallel to the wall and near the boundary layer surface (Y/D = 0.026, $Y/\theta_0 = 0.21$) confirm that the low momentum fluid near the wall downstream of the injection hole is lifted by the CRVP along the spanwise centerline, while higher momentum fluid outboard of the SFD region is pulled inward (see Figures 6 and 7). This is consistent with both the magnitudes and directions of the skin friction vectors determined using FISF. The SFD can therefore be considered an imprint of the CRVP on the surface.

To explain the difference in the SFD between the co- and counter-flow geometries the lateral jet spreading and trajectory must be considered. The counter-flow plenum jet spread angle is on average

3.5° wider than the co-flow plenum and has a lower trajectory (see Hale, 1999). Figure 6 shows that although the jet issues at M = 1.0 for both plenum configurations, the trajectory for the co-flow case is significantly higher than that for the counter-flow because of the "jetting" at the trailing edge of the hole in the former. Furthermore, the PIV data show that the fluid immediately downstream and outboard of the injection hole contains the highest momentum (see Figure 7). This high momentum fluid is further outboard of the injection hole for the counter-flow plenum due to the greater lateral spreading. The higher lateral spreading and lower trajectory of the counter-flow plenum is associated with a weaker or less coherent CRVP.

A potential flow analysis of a pair of counter-rotating vortices above a wall indicates that the pressure distribution on the wall is more dependent upon the distance of the vortices from the wall (a) than their strength; i.e. a pair of weaker vortices close to the wall induces a more severe wall pressure gradient than a stronger vortex pair further from the wall. The expressions for velocity along the wall and between the vortices, and the pressure gradient are given in equations (2) through (4). The nomenclature is defined in Figure 8.

$$v(Z=0) = \frac{b\Gamma}{\pi}\left(\frac{1}{(Y+a)^2+b^2} - \frac{1}{(Y-a)^2+b^2}\right) \quad (2)$$

$$w(Y=0) = \frac{a\Gamma}{\pi}\left(\frac{1}{a^2+(Z+b)^2} - \frac{1}{a^2+(Z-b)^2}\right) \quad (3)$$

$$\frac{\partial p}{\partial Z} = \frac{16\rho\Gamma^2 a^2 b^2 Z}{\pi}\left(\frac{(Z-a)(Z-b)(b^2+3Z^2+2a^2)+a^4}{((Z+b)^2+a^2)^3((Z-b)^2+a^2)^3}\right) \quad (4)$$

The CRVP for the counter-flow plenum is weaker, yet closer to the wall and thus causes a wider stagnation region between the vortices. The co-flow plenum case has a smaller impact on the wall pressure distribution and thus the SFD is not as prominent. See Figure 9 for a schematic showing how the SFD is produced by a low trajectory CRVP in a JICF.

Due to space limitations, the effect of injection angle and blowing ratio are omitted. However, the results for the 35° injection hole and blowing ratio of 0.5 are similar to those presented here. The SFD is present in both the 35° injection hole case and the blowing ratio of 0.5. However, the SFDs are less pronounced for the 35° injection hole geometry.

CONCLUSIONS

The effect of plenum feed direction on the surface skin friction coefficient has been analyzed for a row of jets issuing into a crossflow. The dominant features of the shear stress for the 90° injection hole geometry are: the low skin friction directly upstream of the holes caused by a local 3-dimensional separation, the high skin friction around the holes as the flow accelerates around the jet, the recirculating region immediately downstream of the

jet, and the skin friction deficit that persists far downstream in the wake of the jet.

The plenum feed direction was found to have a significant effect on the SFD, with the counter-flow plenum geometry having the most pronounced deficit region. The SFD is an imprint of the CRVP on the boundary layer plate. The counter-flow plenum geometry has a weaker and less coherent CRVP, which causes increased lateral spreading and lower trajectory. The vortex/surface interaction is stronger than with the co-flow plenum however, due to its proximity.

REFERENCES

Adrian, R.J., 1991, "Statistical Properties of Particle Image Velocimetry Measurements in Turbulent Flow," *Laser Anemometry in Fluid Mechanics vol III* ed R Adrian *et al.* (Lisbon: Ladoani Instituto Superior Tecnico) pp 115-129.

Berhe, M.K. and Patankar, S.V., 1996, "A Numerical Study of Discrete-Hole Film Cooling," *ASME Paper 96-WA/HT-8*.

Brundage, A.L., Plesniak, M.W., and Ramadhyani, S., 1999, "Influence of Coolant Feed Direction and Hole Length on Film Cooling Jet Velocity Profiles," *ASME Paper 99-GT-035*.

Burd, S.W. and Simon, T.W., 1998a, "Measurements of Discharge Coefficients in Film Cooling," *ASME Paper 98-GT-009*.

Burd, S.W. and Simon, T.W., 1998b, "Turbulence Spectra and Length Scales Measured in Film Coolant Flows Emerging from Discrete Holes," *ASME Paper 96-WA/HT-7*.

Driver, D.M., 1997, "Application of Oil-film Interferometry Skin-Friction to Large Wind Tunnels," *AGARD CP-601*, Paper no. 25.

Fric, T.F. & Roshko, A., 1994, "Vortical Structure in the Wake of a Transverse Jet," *Journal of Fluid Mechanics*, 279, pp 1-47.

Hale, C.A., 1999, "Short Hole Film Cooling Hydrodynamics and Convective Heat Transfer in the Near-hole Region," *Ph.D. Thesis*, School of Mechanical Engineering, Purdue University.

Hale, C.A., Plesniak, M.W., and Ramadhyani, S., 2000, "Structural Features and Surface Heat Transfer Associated with a Row of Short-Hole Jets in Crossflow," *International Journal of Heat and Fluid Flow*, 21, pp 542-553.

Hale, C.A., Plesniak, M.W., and Ramadhyani, S., 1999, "Structural Features and Surface Heat Transfer Associated with a Row of Short-Hole Jets in Crossflow," *Proceedings of Turbulence and Shear Flow Phenomena 1999*, S. Banerjee and J.K. Eaton, eds. Begell House, Inc., NY, pp 691-696.

Holdeman, J. D., 1993, "Mixing of Multiple Jets with a Confined Subsonic Crossflow," *Progress in Energy and Combustion Science*, 19, pp 31-70.

Margason, R.J., 1993, "Fifty Years of Jet in Cross Flow Research," *AGARD-CP-534*.

Monson, D.J. & Mateer, G.G., 1993, "Boundary-Layer Transition and Global Skin Friction

Measurements with an Oil-Fringe Imaging Technique," *SAE 932550, Aerotech '93*, Costa Mesa, CA.

Morton, B.R. and Ibbetson, A., 1996, "Jets Deflected in a Crossflow," *Experimental Thermal and Fluid Science*, **12**, pp 112-113.

Simoneau, R.J. & Simon, F.F., 1993, "Progress Towards Understanding and Predicting Heat Transfer in the Turbine Gas Path," *International Journal of Heat and Fluid Flow*, **14**, No.2, pp 106-128.

Thole, K.A., Gritsch, M., Schulz, A., and Wittig, S., 1997, "Effect of a Crossflow at the Entrance to a Film-Cooling Hole," *Journal of Fluids Engineering*, **119**, pp 533-540.

Westerweel, J., 1993, "Digital Particle Image Velocimetry – Theory and Application," *PhD Thesis*, Technical University of Delft.

White, F.M., 1991, Viscous Fluid Flow, 2nd. Ed., McGraw Hill Inc., NY.

Willert, C. and Gharib, M., 1991, "Digital Particle Image Velocimetry," *Experiments in Fluids*, **10**, pp 181-193.

Wittig, S., Schulz, A., Gritsch, M., and Thole, K.A., 1996, "Transonic Film-Cooling Investigations: Effects of Hole Shapes and Orientations," *ASME Paper 96-GT-222*.

Wolochuck, M.C., Plesniak, M.W., and Braun, J.E., 1994, "Evaluation of Vortex Shedding Flow Meters for HVAC Applications," *Purdue University Report ME-TSPC/HERL-TR-94-1*.

Zilliac, G.G., 1996, "Further Developments of the Fringe-Imaging Skin Friction Technique," *NASA TM-110425*.

Zilliac, G.G., 1999, "The Fringe-Imaging Skin Friction Technique," *NASA/TM-1999-208794*.
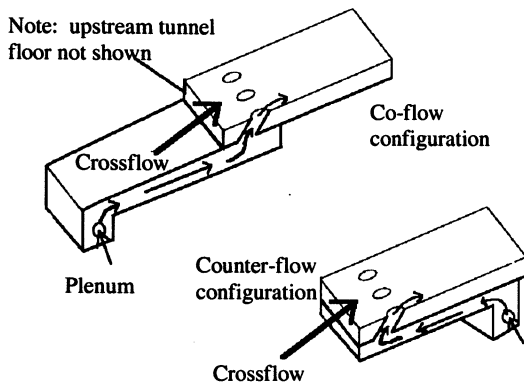
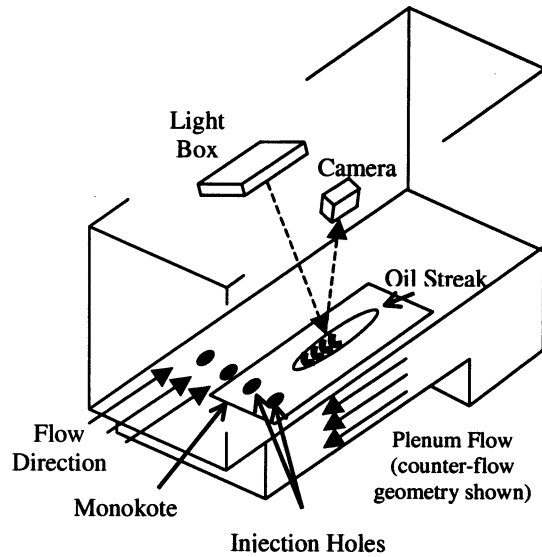Figure 1: Schematic of Boundary Layer Plate, Jets and Plenum
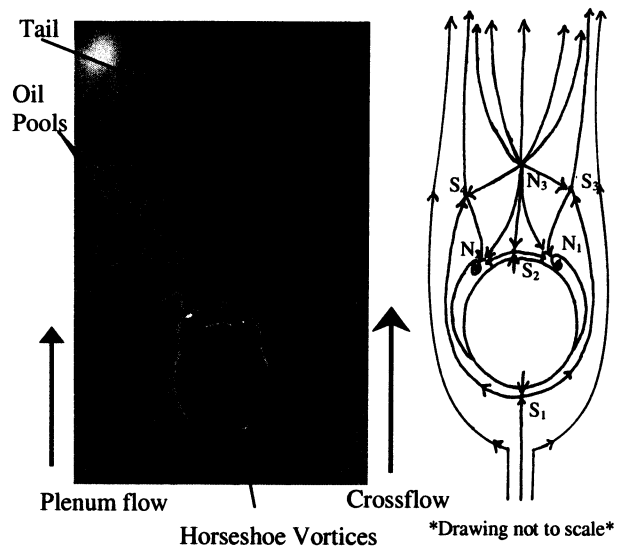

Figure 2: Schematic of FISF Apparatus

Figure 3: Surface Streaks and Topology Surrounding Interior Jet for 90° Short Injection Hole with Co-flow Plenum at M = 1.0 from Hale et al. (2000)
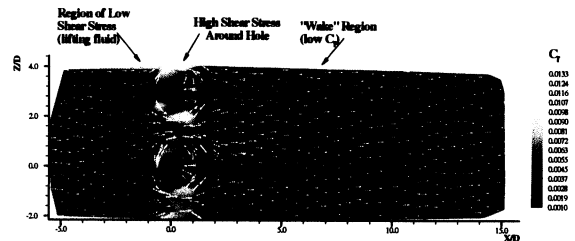

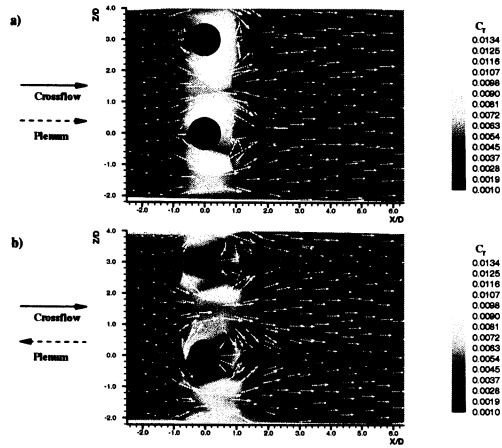Figure 4: Skin Friction Distribution Around JICF, Counter-flow Plenum, 90° Injection, L/D = 0.66, M=1.0

151

Figure 5: Skin Friction Distribution Around JICF, a) Co-flow Plenum, 90° Injection, L/D = 0.66, M=1.0 b) Counter-flow Plenum, 90° Injection, L/D = 0.66, M=1.0
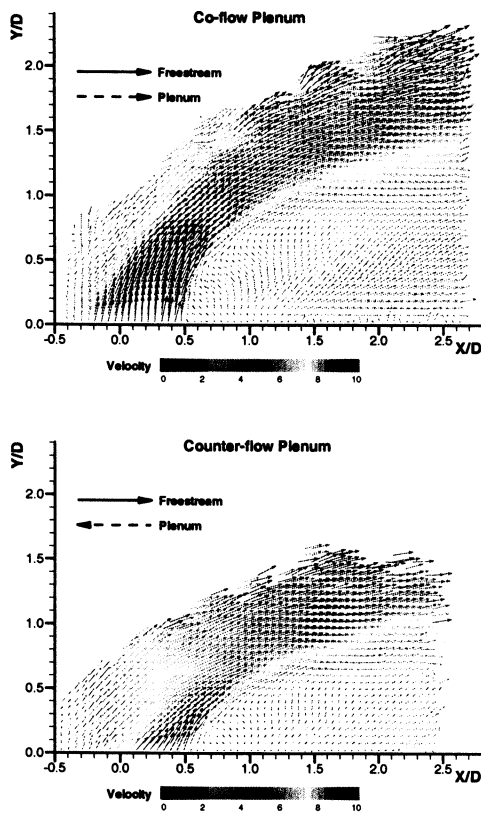

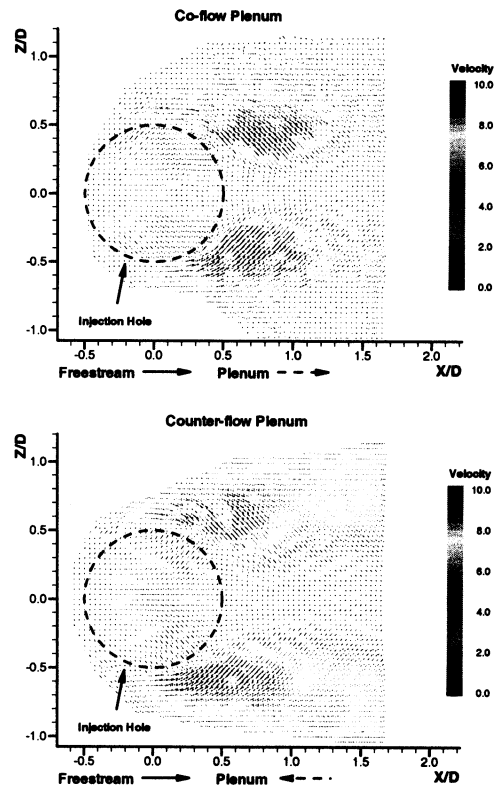Figure 6: Trajectory of a 90° JICF at M = 1.0, Z = 0 a) Co-flow Plenum b) Counter-flow Plenum

Figure 7: Velocity Distribution of JICF at Y/D = 0.04, a) Co-flow Plenum, 90° Injection, L/D = 0.66, M=1.0 b) Counter-flow Plenum, 90° Injection, L/D = 0.66, M=1.0
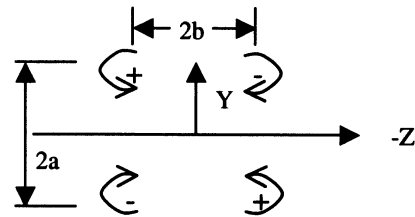

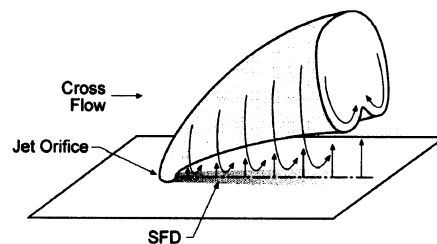Figure 8: Schematic of Potential Flow Analysis for a CRVP Above a Wall

Figure 9: Schematic of JICF Imprint on the Wall, Resulting in SFD Region

152